Nanoscale Res Lett (2009) 4:694–698
DOI 10.1007/s11671-009-9299-5

NANO EXPRESS

# Synthesis and Characterization of Tin Disulfide ($SnS_2$) Nanowires

**Ya-Ting Lin · Jen-Bin Shi · Yu-Cheng Chen · Chih-Jung Chen · Po-Feng Wu**

Received: 7 October 2008 / Accepted: 24 March 2009 / Published online: 5 April 2009


**Abstract** The ordered tin disulfide ($SnS_2$) nanowire arrays were first fabricated by sulfurizing the Sn nanowires, which are embedded in the nanochannels of anodic aluminum oxide (AAO) template. $SnS_2$ nanowire arrays are highly ordered and highly dense. X-ray diffraction (XRD) and corresponding selected area electron diffraction (SAED) patterns demonstrate the $SnS_2$ nanowire is hexagonal polycrystalline. The study of UV/Visible/NIR absorption shows the $SnS_2$ nanowire is a wide-band semiconductor with three band gap energies (3.3, 4.4, and 5.8 eV).

**Keywords** Nanomaterials · $SnS_2$ · Nanowire · AAO · Template

## Introduction

In recent years, one-dimensional (1-D) nanostructural materials have been attractive due to their physical and chemical properties. These nanostructures in particular show results in electronics [1], magnetic [2], optics, etc., that have great potential applications in the next generation of nanodevices [3]. Anodic aluminum oxide (AAO) template-based assembling has been widely applied in recent years to produce nanowires with extremely long length and high aspect ratio, and it also provides a simple, rapid, and cheap way for fabricating nanowires as aligned arrays [4].

Tin disulfide ($SnS_2$) is an n-type semiconductor with hexagonal cadmium iodide ($CdI_2$) structure. It is composed of sheets of tin atoms sandwiched between two close-packed sheets of sulfur atoms [5]. Single crystal and polycrystalline films of $SnS_2$ have shown optical band gaps in the range of 2.12–2.44 eV [6]. As an important member of the IV–VI group semiconductors, $SnS_2$ is a possible choice in solar cells and optoelectronic devices [7]. A variety of methods have been developed into synthesized $SnS_2$ nanoparticles, films, and crystals. $SnS_2$ nanoparticles were synthesized through the microware plasma process either by the reaction between chloride or carbonyl of tin and $H_2S$ [8]. The films of $SnS_2$ were prepared by chemical deposition from an acidic medium solution containing $Sn^{4+}$ ions [9]. Single crystals of $SnS_2$ have been grown by the vapor phase [10]. In addition, $SnS_2$ nanocrystallites with hexagon flake shape were synthesized by a hydrothermal reaction between $SnCl_4 \cdot 5H_2O$ and $(NH_2)_2CS$ [11]. $SnS_2$ nanobelts were produced from $SnCl_2 \cdot 2H_2O$ and $Na_2S$ by a thioglycollic acid (TGA) assisted hydrothermal method [12]. However, $SnS_2$ nanowires are fabricated within AAO template synthesis, using the electrodeposition and sulfurizing methods that are not yet reported.

For this purpose, we report a new synthesis method for semiconductor $SnS_2$ nanowires. Pure metal Sn is electrodeposited in the nanochannels of the AAO template. Sn nanowires are sulfurized in the S atmosphere to form $SnS_2$ nanowires. According to past research, our first successful fabrication attempt was sulfurizing the Sn nanowires that were electrodeposited in the AAO template and studying its properties.

Y.-T. Lin (✉) · Y.-C. Chen · C.-J. Chen · P.-F. Wu
The Graduate Institute of Electrical and Communications Engineering, Feng Chia University, 100, Wen-Hwa Rd, Seatwen, Taichung 40724, Taiwan
e-mail: p9431597@fcu.edu.tw

J.-B. Shi
Department of Electronic Engineering, Feng Chia University, Taichung 40724, Taiwan

## Experimental Details

### Preparation of AAO Template

The AAO template used in our experiment was prepared by a two-step anodization process as described previously [13]. Briefly, high purity aluminum sheet (99.9995%) was first anodized at constant voltage in the sulfuric acid solution for 3 h. After anodization, the anodized Al sheet was put into an acid to completely remove the porous layer. Then, the AAO template can be fabricated by repeating the anodization process under the same conditions of the first step anodization. The AAO template was obtained by etching away the underlying aluminum substrates with a mercuric chloride solution. The transparent AAO template was immersed in a phosphoric acid solution to widen the nanochannels. After this process, the diameter of the nanochannel was about 40 nm.

### Preparation of $SnS_2$ Nanowires

In order to prepare Sn nanowires, a platinum (Pt) film was deposited by vacuum evaporation onto one surface of the AAO template to provide a conductive contact. The Sn nanowires were electrodeposited in the pore of the nanochannels of AAO template under constant voltage, using an electrolyte containing $SnSO_4$ and distilled water. After washing with distilled water and air drying, the AAO template with Sn nanowires was put into a glass tube with the pure S powder together. The glass tube was evacuated by using a pump, and it was placed into the furnace. The samples were then heated from room temperature (heating rate: 5 °C/min) to 500 °C and kept at this temperature for 10 h to completely sulfurize the Sn nanowires. It is expected that S atoms would react with the metal Sn to form $SnS_2$. After the reaction was terminated, the furnace was naturally cooled down to room temperature and $SnS_2$ nanowires were completely formed after sulfurization.

### Characterization of $SnS_2$ Nanowires

The morphology and microstructure of the as-prepared $SnS_2$ nanowire arrays were characterized by field emission scanning electron microscopy/energy dispersive spectrometer (FE-SEM/EDS, HITACHI S-4800). The identification of the crystallization and phase structure were analyzed by X-ray diffraction (XRD, SHIMADZU XRD-6000) utilizing Cu Kα radiation. More details about the microstructure of the $SnS_2$ nanowires were investigated by the high-resolution transmission electron microscopy/corresponding selected area electron diffraction (HR-TEM/SAED, JEOL JEM-2010). For HR-TEM and SAED analysis, the $SnS_2$ nanowires were dispersed in ethanol and vibrated for few minutes. Then, a few drops of the resulting suspension were dripped onto a copper grid. For optical analysis, the AAO template was dissolved by NaOH solution at room temperature and was washed with distilled water to expose freely nanowires of $SnS_2$. After the $SnS_2$ nanowires are absolutely dispersed in distilled water using a supersonic disperser, the absorption spectra of the $SnS_2$ nanowires were measured on an UV/Visible/NIR spectrophotometer (HITACHI U-3501).

## Results and Discussion

### Morphology of AAO Template and $SnS_2$ Nanowires

The morphology of the as-synthesized product was examined by FE-SEM. Typical FE-SEM morphology (Fig. 1a) shows the pores on the AAO template had a uniform size and were arranged in a honeycomb hexagonal structure. Figure 1b shows the pure Sn nanowire arrays in the pore of nanochannels of AAO template. It shows the length of Sn nanowires is about 5 μm. Figure 1c shows the $SnS_2$ nanowires embedded in an AAO template. It reveals the aspect ratio (length/diameter) of $SnS_2$ nanowires around 125. When the sulfurization temperature was fixed at 500 °C, the formation of $SnS_2$ nanowires was confirmed by sulfurization up to 10 h. From the high-magnification FE-SEM micrograph (Fig. 1d), $SnS_2$ nanowires with the diameter of about 40 nm can be clearly observed. The chemical composition of the $SnS_2$ nanowires was investigated by EDS. Figure 1e reveals EDS spectra of $SnS_2$ nanowires arrays, indicating only aluminum, oxygen, tin, and sulfur were present, and that there was no contamination by other elements. Quantitative analysis reveals the atomic ratio of Sn to S with 33.92:66.08 is close to 1:2, indicating the $SnS_2$ nanowires are well-crystallized, and they are in good agreement with the XRD results. In order to investigate the morphology of the $SnS_2$ nanowires, the AAO template was completely removed in NaOH for 15 min to expose them, followed by thoroughly rinsing with distilled water. Figure 1f reveals the $SnS_2$ nanowires with diameter of about 40 nm detached from the AAO template. The individual $SnS_2$ nanowires were almost the same diameter of the AAO template. The geometrical characteristics of the $SnS_2$ nanowires could be controlled by choosing the proper type of AAO template.

### Crystal Structures of $SnS_2$ Nanowires

Figure 2 shows the X-ray diffraction (XRD) spectra of the as-prepared $SnS_2$ nanowires without AAO template, which makes the crystal structure of the $SnS_2$ nanowires convenient for characterization. It can be seen that there are no

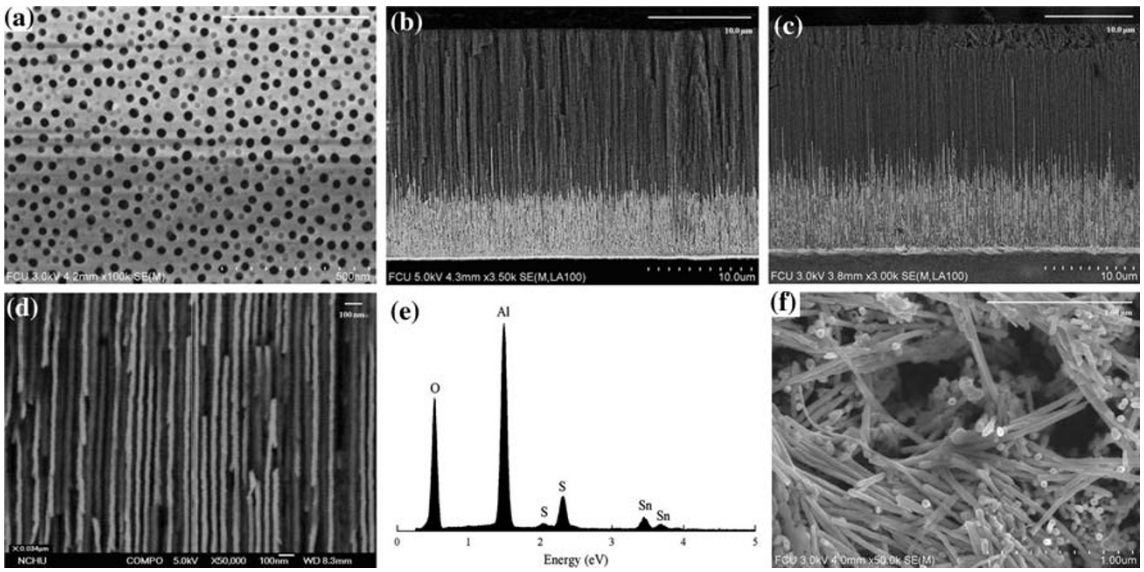


**Fig. 1** FE-SEM micrographs of **a** top view of the AAO template, **b** cross-section view of Sn nanowires arrays in the pore of the nanochannels of AAO template, **c** cross-section view of $SnS_2$ nanowires were embedded in an AAO template, **d** the magnified FE-SEM micrograph of (**c**), **e** EDS spectra of the $SnS_2$ nanowires, and **f** the AAO template was absolutely dissolved by NaOH solution

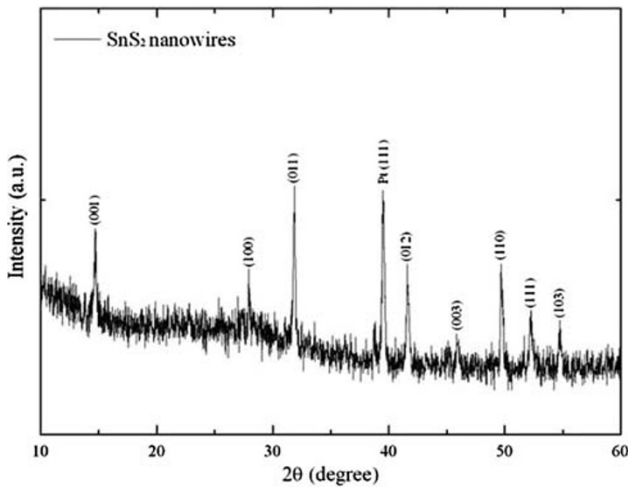


**Fig. 2** X-ray diffraction patterns of $SnS_2$ nanowires without AAO template

peaks of Sn and S after the metal Sn nanowires are sulfurated at 500 °C for 10 h. Furthermore, the Sn peaks totally disappear after sulfuration and the $SnS_2$ peaks appear. The indicated formation of $SnS_2$ in hexagonal crystal phase has a preferred orientation (011), which is in good agreement with the reported values (JCPDS Card no.83-1705). Metal oxides such as $SnO_2$ nanowires have been prepared by oxidation of metal Sn nanowires, and it is generally accepted that the chemical properties of oxygen and sulfur are similar to each other. Hence, the technique used here for formation of $SnS_2$ is understandable. The formation mechanism of $SnS_2$ nanowires with the reaction equation can be expressed as follows:

$$Sn^{4+} + 2S^{-} \rightarrow SnS_2 \quad (1)$$

in which the S atoms would react with metal Sn atoms at high temperatures to form $SnS_2$ nanowires. Since the reaction rates of S and Sn atoms are mainly dominated by time and temperature, long periods and high temperatures of the sulfurization process were needed to prepare the fine crystalline $SnS_2$ nanowires. When the sulfurization time was fixed for 10 h, the formation of $SnS_2$ nanowires were confirmed by sulfurization at a temperature of 500 °C.

Detailed information on the microstructure of as-prepared $SnS_2$ nanowires was obtained by HR-TEM. Low-magnification HR-TEM image (Fig. 3a) illustrates the numerous $SnS_2$ nanowires. Figure 3b reveals the HR-TEM image of an individual $SnS_2$ nanowire. The diameter of the nanowire is about 40 nm. Nevertheless, the grain size of the $SnS_2$ nanowire cannot be clearly observed. In Fig. 3c, the corresponding SAED pattern of an individual nanowire exhibits a polycrystalline. Moreover, the concentric diffraction rings could be indexed outward as (011), (001), (012), and (110) lattice planes of hexagonal $SnS_2$. The HR-TEM image (Fig. 3d) shows a single nanowire with the lattice spacing of about 0.2777 nm, which corresponds to (011) plane of $SnS_2$.

## Optical Properties of $SnS_2$ Nanowires

Figure 4 shows the UV/Visible/NIR absorbance spectra of the as-grown sample recorded in the spectral range 200–900 nm for $SnS_2$ nanowires. Our absorption spectra results of $SnS_2$ nanowires have a very strong absorption peak at

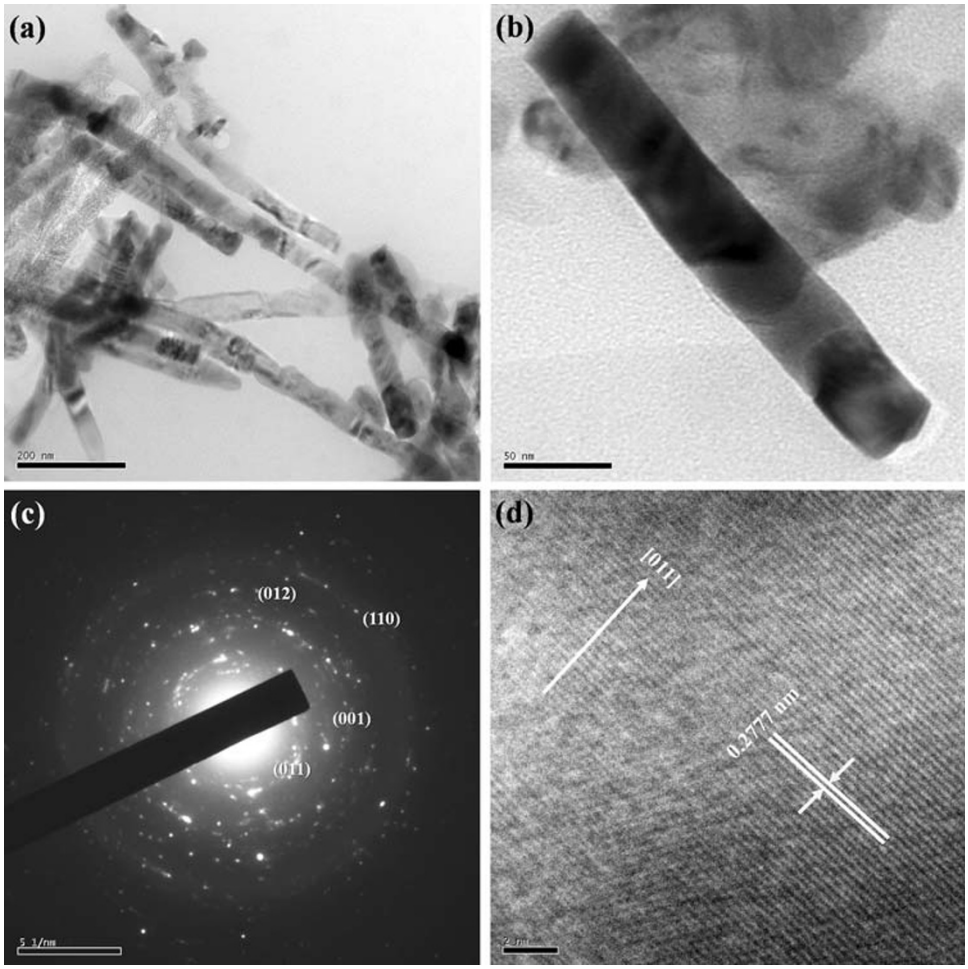


**Fig. 3** **a** The low-magnification HR-TEM image of $SnS_2$ nanowires, **b** the high-magnification HR-TEM image of an individual $SnS_2$ nanowire, **c** SAED pattern of an individual $SnS_2$ nanowire, and **d** HR-TEM image of a single $SnS_2$ nanowire with lattice fringes

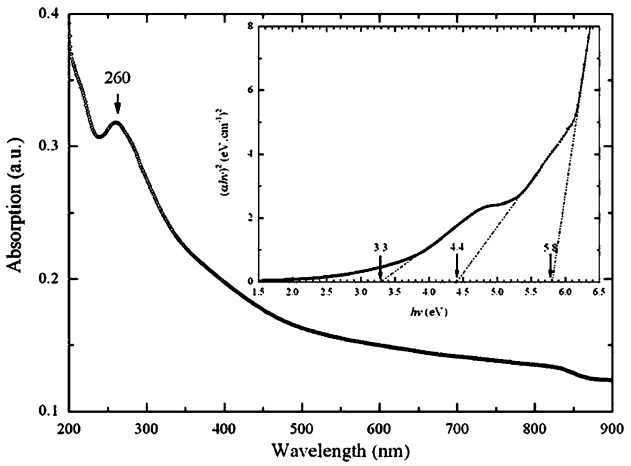


**Fig. 4** UV/Visible/NIR absorption spectra with $SnS_2$ nanowires and $(\alpha hv)^2$ versus $hv$ plot (inset)

260 nm, no other peaks can be observed. We infer the absorption peak at 260 nm in ultraviolet region is due to the phase of the tin disulfide ($SnS_2$). SnS was not observed because it has a strong absorption onset around 980 nm of direct band gap and a weaker absorption edge near 1100 nm of the indirect band gap [14]. This result proves our sulfured nanowires are $SnS_2$ phase, and it is in accordance with our XRD results. To determine the band gap energy ($E_g$) of the $SnS_2$ nanowires, the dependence of absorption coefficient ($\alpha$) on the photon energy equation is given as follows [15]:

$$\alpha hv = A\left(hv - E_g\right)^m \quad (2)$$

where $hv$ is the photon energy, $E_g$ the band gap energy, and A is the constant having separate values for different transitions. The values of $m$ for allowed direct, allowed indirect, forbidden direct, and forbidden indirect transition are 1/2, 2, 3/2, and 3, respectively. This equation gives band gap ($E_g$) when straight portion of $(\alpha hv)^{1/m}$ versus $hv$ plots are extrapolated to the point $\alpha = 0$. However, $m =$ 3/2, 2, and 3, the band gap energies were found to be a negative number which is not reasonable in physics. Relationship fitting to the absorption spectra of $SnS_2$ as $m = 1/2$, which means these nanowires are allowed direct transition. As $m = 1/2$, the $(\alpha hv)^2$ versus $hv$ plot is shown in the inset in Fig. 4, exhibiting a linear relationship at 3.9–4.75, 5.4–6.1, and 6.2–6.35 eV, respectively. The band gap

energies of 40 nm $SnS_2$ nanowires are estimated to be 3.3, 4.4, and 5.8 eV by the extrapolation of relation. According to the most recent study about the optical characteristics of the $SnS_2$ films, absorbance spectra were recorded in the spectral range 350–800 nm. Deshpande et al. [16] recently reported the band gap energy of the allowed direct transitions at 2.2 eV in the $SnS_2$ films with average grain sizes of: 180–220 nm. The band gap energies of $SnS_2$ nanowires were higher than that of $SnS_2$ films. Panda et al. [17] observed the direct optical transition and the band gap energy was 3.5 eV with crystalline nanoparticles of 15 nm annealed at 150 °C for 1 h. In this study, the band gap energy of the allowed direct transitions at 3.3 eV of $SnS_2$ nanowires with 40 nm diameter is agreeable to those obtained of Panda et al. Our band gap energy (3.3 eV) of $SnS_2$ nanowires is reasonable when compared with the band gap energy (2.2-3.5 eV) of $SnS_2$ films. Wang et al. [18] reported the absorption spectra were recorded in the spectral range under 350 nm. They observed the emission or excitation bands of $SnS_2$ nanocrystallites, which are associated with the transition between those sub-bands. Those bands of $SnS_2$ nanocrystallites may be associated with the presence of defect either interface or interior. Our band gap energies (4.4 and 5.8 eV) of $SnS_2$ nanowires are probably a result of sub-band in the electronic structure. Chang et al. reported $SnS_2$ nanotubes could be a one-dimensional sensor material for $NH_3$ detection, indicating that $SnS_2$ nanowires may be suitable for $NH_3$ sensor applications [19]. This can be explained by the calculated binding energies for a $NH_3$ molecule on the $SnS_2$, which are very close to those obtained previously in calculations of $NH_3$ adsorption onto a carbon nanotube [20]. In the future, we will study the energy jump of physical phenomenon, development and applications in gas sensor and solar cell.

## Conclusions

$SnS_2$ nanowires arrays have been successfully fabricated within template synthesis by using the electrodeposition and sulfurizing methods. The results show $SnS_2$ nanowires have high wire packing densities with uniform wire diameters and lengths of about 40 nm and 3–5 μm, respectively. In XRD results, after sulfuring the Sn nanowire at 500 °C for 10 h, the sulfured nanowires have $SnS_2$ phase and a preferred orientation (011). The analysis of the HR-TEM/SAED reveals the $SnS_2$ nanowire is polycrystalline. The $SnS_2$ nanowires show three band gap energies (3.3, 4.4, and 5.8 eV) and exhibit a linear relationship at 3.9–4.75, 5.4–6.1, and 6.2–6.35 eV, respectively as $m = 1/2$. The absorption spectra of nanowires contain three spectral intervals with the shapes typical for direct allowed interband transitions with the effective bandgaps.

**Acknowledgments** The research was supported by the National Science Council of R.O·C. under grant No. NSC-96-2122-M-035-003-MY2.

## References

1. G. Yi, W. Schwarzacher, Appl. Phys. Lett. **74**, 1746 (1999). doi:10.1063/1.123675
2. C.A. Ross, M. Hwang, M. Shima, H.I. Smith, M. Farhoud, T.A. Savas et al., J. Magn. Magn. Mater. **249**, 200 (2002). doi:10.1016/S0304-8853(02)00531-0
3. M.P. Zach, K.H. Ng, R.M. Penner, Science **290**, 2120 (2000). doi:10.1126/science.290.5499.2120
4. Q.H. Zhang, Z.J. Chang, M.F. Zhu, X.M. Mo, D.J. Chen, Nanotechnology **18**, 115611 (2007). doi:10.1088/0957-4484/18/11/115611
5. D.L. Greenaway, R. Nitsche, J. Phys. Chem. Solids **26**, 1445 (1965). doi:10.1016/0022-3697(65)90043-0
6. G. Said, P.A. Lee, Phys. Status Solidi, A Appl. Res. **15**, 99 (1973). doi:10.1002/pssa.2210150111
7. S. Polarz, B. Smarsly, C. Goltner, M. Antonietti, Adv. Mater. **12**, 1499 (2000). doi:10.1002/1521-4095(200010)12:20<1503::AID-ADMA1503>3.0.CO;2-X
8. D. Vollath, D.V. Szab'o, Acta Mater **48**, 953 (2000). doi:10.1016/S1359-6454(99)00395-X
9. K. Matsumoto, S. Kaneko, Thin Solid Films **121**, 227 (1984). doi:10.1016/0040-6090(84)90304-3
10. C.D. Lokhande, J. Phys. D Appl. Phys. (Berl) **23**, 1703 (1990)
11. C.R. Wang, K.B. Tang, Q. Yang, Y.T. Qian, C.Y. Xu, Chem. Lett. **12**, 1294 (2001). doi:10.1246/cl.2001.1294
12. Y.J. Ji, H. Zhang, X.Y. Ma, J. Xu, D.E. Yang, J. Phys. Condens. Matter **15**, 661 (2003). doi:10.1088/0953-8984/15/44/L02
13. J.B. Shi, Y.C. Chen, C.W. Lee, Y.T. Lin, C. Wu, C.J. Chen, Mater. Lett. **62**, 15 (2008). doi:10.1016/j.matlet.2007.04.060
14. E.C. Greyson, J.E. Barton, T.W. Odom, Small **2**, 368 (2006). doi:10.1002/smll.200500460
15. G. Burns, *Solid State Physics* (Academic Press, Orlando, 1985)
16. N.G. Deshpande, A.A. Sagade, Y.G. Gudage, C.D. Lokhande, R. Sharma, J. Alloys Compd. **436**, 421 (2007). doi:10.1016/j.jallcom.2006.12.108
17. S.K. Panda, A. Antonakos, E. Liarokapis, S. Bhattacharya, S. Chaudhuri, Mater. Res. Bull. **42**, 576 (2007). doi:10.1016/j.materresbull.2006.06.028
18. C.R. Wang, K.B. Tang, Q. Yang, Y.T. Qian, Chem. Phys. Lett. **357**, 371 (2002). doi:10.1016/S0009-2614(02)00495-5
19. H. Chang, E. In, K.J. Kong, J.O. Lee, Y. Choi, B.H. Ryu, J. Phys. Chem. B **109**, 30 (2005). doi:10.1021/jp044983o
20. H. Chang, J.D. Lee, S.M. Lee, Y.H. Lee, Appl. Phys. Lett. **79**, 3863 (2001). doi:10.1063/1.1424069